



**CHALMERS**  
UNIVERSITY OF TECHNOLOGY

## **Flame folding and conditioned concentration profiles in moderately intense turbulence**

Downloaded from: <https://research.chalmers.se>, 2026-04-05 12:19 UTC

Citation for the original published paper (version of record):

Lipatnikov, A., Sabelnikov, V. (2022). Flame folding and conditioned concentration profiles in moderately intense turbulence. *Physics of Fluids*, 34(6). <http://dx.doi.org/10.1063/5.0095866>

N.B. When citing this work, cite the original published paper.

# Flame folding and conditioned concentration profiles in moderately intense turbulence

Andrei N. Lipatnikov<sup>a,\*</sup>, Vladimir A. Sabelnikov<sup>b</sup>

<sup>a</sup>*Department of Mechanics and Maritime Sciences, Chalmers University of Technology, Gothenburg SE-412 96, Sweden*

<sup>b</sup>*ONERA – The French Aerospace Laboratory, F-91761 Palaiseau, France*

*\*Corresponding author, lipatn@chalmers.se*

## Abstract

While the flamelet paradigm offers the opportunity to simplify computations of mean species concentrations in turbulent flames, a widely accepted criterion of the validity of this paradigm has not yet been elaborated. In this regard, different physical mechanisms are discussed, and flame folding is one of them. The present work aims at exploring the eventual influence of flame folding on the local flame structure in a turbulent flow. For this purpose, a new diagnostic technique was applied to processing complex-chemistry direct numerical simulation data obtained earlier from a lean hydrogen-air turbulent flame [H.L. Dave and S. Chaudhuri, *J. Fluid Mech.* 884, A46 (2020)]. The technique consists of counting crossing numbers  $N_f$  for a cold boundary of the local reaction zone and a ray normal to the mean flame brush, followed by analyzing statistics sampled from rays characterized by  $N_f \geq 3$ . More specifically, profiles of species mole fractions, temperature, heat release rate, and species production rates, conditioned to combustion progress variable and either  $N_f$  or axial distance  $\Delta x$  between two neighboring reaction zones, are sampled and compared with the counterpart profiles obtained from the laminar flame. Results show that these doubly conditioned profiles are close to each other for various crossing numbers or for various axial distances even if the distance is as small as half laminar flame thickness. The lack of a substantial effect of the crossing number or the axial distance on the doubly conditioned profiles implies that small-scale flame folding does not limit the validity of the flamelet paradigm.

**Keywords:** Turbulent combustion; Flame folding; Conditioned profiles; Hydrogen

## I. INTRODUCTION

Until recently, the focus research into premixed turbulent combustion was placed on the influence of turbulence on a burning rate<sup>1-5</sup> and the influence of a flame on turbulence.<sup>6-10</sup> Currently, due to the threat of global warming, new challenges arise. In particular, an urgent need for development of ultra clean burning technologies calls for efficient methods capable

30 for predicting emissions from combustion engines. From this perspective, the flamelet  
31 paradigm<sup>11</sup> is very attractive, because it offers the opportunity to significantly simplify  
32 computations of mean concentrations of various species in flames. Initially, this paradigm was  
33 developed for modeling weakly turbulent combustion. Recent experimental and numerical  
34 studies reviewed by Driscoll et al.,<sup>12</sup> as well as the latest measurements<sup>13</sup> and simulations,<sup>14-25</sup>  
35 indicate that premixed flames locally retain the scalar structure of laminar flames even in  
36 intense turbulence. In particular, Prof. Pfitzner et al.<sup>21-25</sup> substantially advanced the flamelet  
37 approach over the past three years. These recent results extend the domain of applicability of  
38 the flamelet paradigm, but boundaries of this domain are still not known.

39 For instance, flame folding followed by flame-flame interactions is expected to play a more  
40 important role with increasing turbulent intensity, thus, reducing predictive capabilities of the  
41 flamelet approach in intense turbulence. However, such quite natural expectations should  
42 nevertheless be probed. While flame folding and flame-flame interactions were numerically  
43 explored in the literature,<sup>25-30</sup> the focus of the earlier studies was placed on turbulent burning  
44 rate, flame surface area, or probability density functions. Since these quantities were shown  
45 to be substantially affected by flame folding and flame-flame interactions, one could also  
46 expect substantial influence of the discussed phenomena on the local scalar structure of the  
47 interacting flames. However, the present authors are not aware of research into such an  
48 influence. Therefore, a reasonable agreement<sup>12-20</sup> between conditioned profiles of species  
49 concentrations or temperature, extracted from highly turbulent flames, with results of  
50 simulations of laminar flames could be attributed not only to (i) a minor role played by flame  
51 folding and flame-flame interactions under conditions of the cited studies, but also to (ii)  
52 statistically weak sensitivity of local flame structure to these phenomena. Even if the latter  
53 alternative does not seem to be expected, it should be explored. Since the present authors are

54 not aware of a relevant study, this work aims at filling this knowledge gap by analyzing Direct  
55 Numerical Simulation (DNS) data by Dave et al.<sup>31,32</sup>.

56 In the next section, the DNS attributes and data processing methods are reported. Results  
57 are discussed in Sect. III, followed by conclusions.

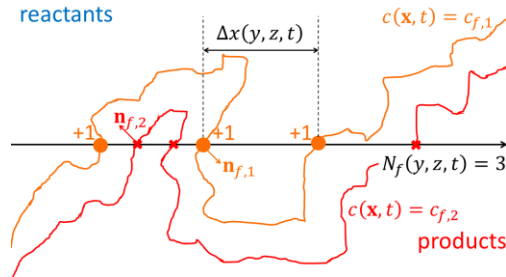
## 58 59 **II. DNS ATTRIBUTES AND PROCESSING METHODS**

60 Since the simulations were already discussed in earlier papers,<sup>14,16,31,32</sup> we will restrict  
61 ourselves to a brief summary of them. A statistically planar, lean H<sub>2</sub>/air flame propagating in  
62 a box was simulated using a detailed chemical mechanism (21 reactions, 9 species) by Li et  
63 al.<sup>33</sup> jointly with the mixture-averaged molecular transport model. To numerically solve  
64 unsteady and three-dimensional compressible continuity, Navier-Stokes, species and energy  
65 transport equations in a parallelepiped ( $19.18 \times 4.8 \times 4.8$  mm) meshed using a uniform grid  
66 of  $960 \times 240 \times 240$  cells, the Pencil code<sup>34</sup> was adopted. Navier-Stokes characteristic  
67 boundary conditions<sup>35</sup> were set at the inlet and outlet. At the transverse sides, boundary  
68 conditions were periodic.

69 Combustion simulations were started at  $t = 0$  by embedding a pre-computed planar laminar  
70 flame into the computational domain at  $x = x_0$ . Subsequently, the flame propagated along the  
71  $x$ -axis against a turbulent flow injected into the computational domain through the inlet (left)  
72 boundary. Before the start of the combustion simulation, homogeneous isotropic turbulence  
73 was generated adopting large-scale forcing in a cube with the fully periodic boundary  
74 conditions and was evolved until a statistically stationary state characterized by Kolmogorov-  
75 Obukhov's 5/3-spectrum was reached.<sup>31</sup> At  $t \geq 0$ , this turbulence was injected into the  
76 computational domain at a constant mean velocity. The turbulence decayed along the  $x$ -axis.

77 Under the simulation conditions (atmospheric pressure, unburned gas temperature  $T_u = 310$   
78 K, and the equivalence ratio  $\Phi = 0.81$ ), the laminar flame speed  $S_L$ , thickness  $\delta_L =$

79  $(T_b - T_u)/\max|\nabla T|$ , and time scale  $\tau_f = \delta_L/S_L$  are equal to 1.84 m/s, 0.36 mm, and 0.20 ms,  
80 respectively. The pre-generated homogeneous isotropic turbulence is characterized<sup>32</sup> by the  
81 rms velocity  $u' = 6.7$  m/s, an integral length scale  $L = 3.1$  mm, an integral time scale  $\tau_t =$   
82  $L/u' = 0.46$  ms, Kolmogorov length scale  $\eta = (v_u^3/\langle\varepsilon\rangle)^{1/4} = 0.018$  mm, Kolmogorov time  
83 scale  $\tau_\eta = (v_u/\langle\varepsilon\rangle)^{1/2} = 0.015$  ms, and turbulent Reynolds number  $Re_t = u'L/v_u = 950$ .  
84 Thus, Karlovitz number and  $Ka = (\delta_L/\eta)^2 = 400$  and Damköhler number  $Da = \tau_t/\tau_f =$   
85 2.35. Here,  $\langle\varepsilon\rangle = \langle 2\nu S_{ij}S_{ij} \rangle$  is the rate of dissipation of turbulent kinetic energy, averaged  
86 over the cube;  $S_{ij} = (\partial u_i/\partial x_j + \partial u_j/\partial x_i)/2$  is the rate-of-strain tensor;  $\nu$  is the kinematic  
87 viscosity of the mixture; the summation convention applies to repeated indexes; subscripts  $u$   
88 and  $b$  designate unburned and burned gas, respectively. Due to the turbulence decay along the  
89 mean flow direction,  $u' = 3.3$  m/s at the leading edge of the mean flame brush, whereas the  
90 turbulence length scales vary weakly between the inlet boundary and the leading edge.



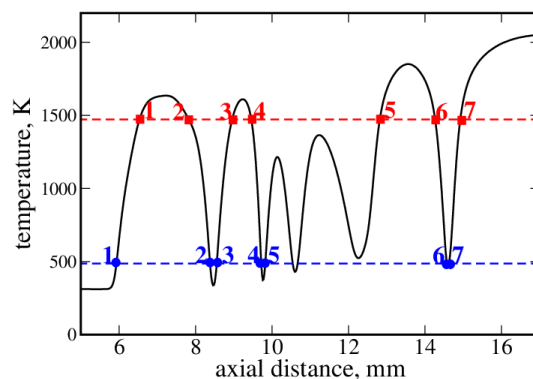
91  
92

**FIG. 1.** Diagnostics of flame folding events.

93 To explore flame folding events and their effects on the local flame structure, the DNS data  
94 were processed as follows. First, at each instant  $t$ , rays  $\{y = y_j, z = z_k\}$  parallel to the  $x$ -axis  
95 and normal to the mean flame brush were drawn from each grid node in the inlet plane to the  
96 outlet plane, see black arrow in Fig. 1. Then, a crossing number  $N_f$  was counted for each ray  
97 and the cold boundary  $c(\mathbf{x}, t) = c_{f,1}$  of the reaction zone, see circles on an orange curve in

98 Fig. 1. Note that if a ray had crossed the cold boundary at least once, the next increase in the  
 99 crossing number was allowed solely when the ray had also crossed the hot boundary  $c(\mathbf{x}, t) =$   
 100  $c_{f,2}$  (the latter events shown in crosses on a red curve in Fig. 1 were not counted in  $N_f$ ).  
 101 Accordingly, (i) even crossing numbers were associated with local flame elements that move  
 102 to the right, i.e., to the product side of the flame brush, and (ii) the largest (for each ray)  
 103 crossing number, i.e.,  $N_f(y, z, t)$ , was an odd number, because  $c(y, z, t) > c_{f,2}$  at the outlet.

104 Results reported in the following were obtained using the temperature-based combustion  
 105 progress variable  $c = (T - T_u)/(T_b - T_u)$ . The boundaries  $c_{f,1} = 0.10$  and  $c_{f,2} = 0.66$  have  
 106 been set using a constraint of  $\dot{\omega}_T(c_{f,1}) = \dot{\omega}_T(c_{f,2}) = 0.5\max\{\dot{\omega}_T(c)\}$ , where  $\dot{\omega}_T(c)$   
 107 designates dependence of Heat Release Rate (HRR) on the combustion progress variable in  
 108 the unperturbed laminar flame. A similar analysis was performed adopting fuel concentration  
 109 to define another combustion progress variable and setting the reaction zone boundaries for  
 110 the local Fuel Consumption Rate (FCR)  $\dot{\omega}_F(\mathbf{x}, t)$  to be equal to half the peak FCR in the  
 111 laminar flame. Since major results obtained using (i) the temperature-based combustion  
 112 progress variable and HRR or (ii) the fuel-based combustion progress variable and FCR are  
 113 similar, we will restrict ourselves to reporting the former results only.



114  
 115 **FIG. 2.** Typical instantaneous axial temperature profile characterized by the largest obtained  
 116  $N_f(y, z, t)$ . Blue circles and red squares show boundaries of local reaction zones.

117 Shown in Fig. 2 is a typical instantaneous axial temperature profile characterized by the  
 118 largest  $N_f(y, z, t) = 7$  found by processing the DNS data. In some cases,  $c_{f,1} = 0.10$  and  
 119  $c_{f,2} = 0.66$  bound thick reaction zones, which have complicated local structures, e.g., see the  
 120 temperature profile between the fifth blue circle and the fifth red square. Such zones appear  
 121 to be particularly difficult to model using the flamelet approach.

122 Figure 2 illustrates also that the number  $N_f(y, z, t)$  depends on the choice of  $c_{f,1}$  and  $c_{f,2}$ .  
 123 Indeed,  $N_f(y, z, t) = 9$  can be obtained by slightly increasing  $c_{f,1}$  and decreasing  $c_{f,2}$  in order  
 124 for each shifted horizontal straight dashed line to cross the local dome centered at  $x \approx 11.5$   
 125 mm twice. Nevertheless, such variations in  $c_{f,1}$ ,  $c_{f,2}$ , and, hence,  $N_f(y, z, t)$  weakly affect  
 126 doubly conditional profiles discussed below and reported later, because these profiles are  
 127 almost the same for different  $N_f(y, z, t)$ , as will be shown in Sect. III.

128 Doubly conditioned single-point scalar mixture characteristics  $\langle \phi | \xi, N_m \rangle$  were sampled  
 129 from grid points characterized by  $|c(\mathbf{x}, t) - \xi_j| < 0.005$  along rays characterized by  
 130  $N_f(y, z, t) = N_m$  at various instants  $t$ . Here,  $\xi_j = 0.01j$  with  $j = 0, \dots, 100$  is a sample  
 131 variable for the instantaneous  $c(\mathbf{x}, t)$ -field and  $\phi$  subsumes mass fraction  $Y_l$  of  $l$  species, the  
 132 rate  $\dot{\omega}_l$  of its production, temperature  $T$ , and HRR. Comparison of the conditional profiles  
 133  $\langle \phi | \xi, N_m \rangle$  sampled at different  $N_m$  offers the opportunity to statistically explore the influence  
 134 of flame folding on the local flame structure.

135 Besides, along each ray characterized by  $N_f(y, z, t) > 1$ , axial distances  $\Delta x(y, z, t)$   
 136 between two rightmost neighboring crossing points  $c(\mathbf{x}, t) = c_{f,1}$  (i.e., axial distances  
 137 between leading edges of two reaction zones that are most close to the outlet boundary, see  
 138 the distance  $\Delta x(y, z, t)$  in Fig. 1 or a small distance between blue circles 6 and 7 in Fig. 2)  
 139 were calculated. Then, doubly conditioned quantities  $\langle \phi | \xi, \Delta_m \rangle$  were sampled along rays

140 characterized by  $\Delta_{m-1} < \Delta x(y, z, t) \leq \Delta_m$  and  $N_f(y, z, t) > 1$  at all instants. Here,  $\Delta_m -$   
 141  $\Delta_{m-1} = \delta_L/2$  and  $\Delta_0 = 0$ . Comparison of the conditional profiles  $\langle \phi | \xi, \Delta_m \rangle$  sampled at  
 142 different  $\Delta_m$  also offers the opportunity to explore the statistical influence of flame folding on  
 143 the local flame structure.

144 The conditional profiles were sampled from 56 snapshots stored, each 5  $\mu$ s over 1.291 ms  
 145  $\leq t \leq 1.566$  ms or  $2.8 \leq t/\tau_t \leq 3.4$ ).

### 146 III. RESULTS AND DISCUSSION

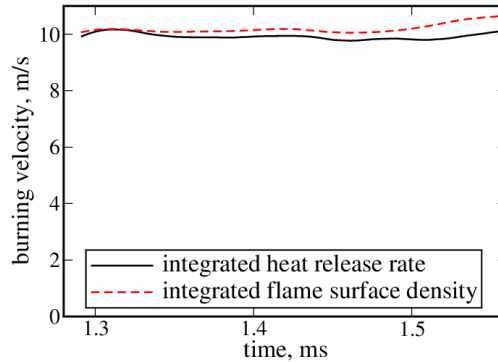
147 Figure 3 compares evolutions of turbulent burning velocities evaluated by integrating the  
 148 HRR expressed in  $\text{g}\cdot\text{K}/(\text{cm}^3\text{s})$  or the flame surface density  $|\nabla c|(\mathbf{x}, t)$  over the computational  
 149 domain  $\Omega$ , i.e.,

$$150 \quad U_t^{HRR}(t) = \frac{1}{\rho_u(T_b - T_u)\Lambda^2} \iiint_{\Omega} \dot{\omega}_T(\mathbf{x}, t) d\mathbf{x}, \quad (1)$$

$$151 \quad U_t^{FSD}(t) = \frac{S_L}{\Lambda^2} \iiint_{\Omega} |\nabla c|(\mathbf{x}, t) d\mathbf{x}. \quad (2)$$

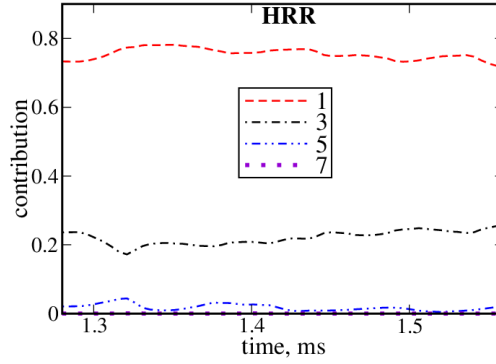
152 Here,  $\rho$  is the density and  $\Lambda$  is the computational domain width. In line with the flamelet  
 153 paradigm,  $U_t^{HRR}(t) \approx U_t^{FSD}(t)$ . At the same time, a large  $U_t^{HRR}(t) > 5S_L$  implies that flame  
 154 folding could substantially affect  $U_t^{HRR}(t)$ .

155



156  
 157

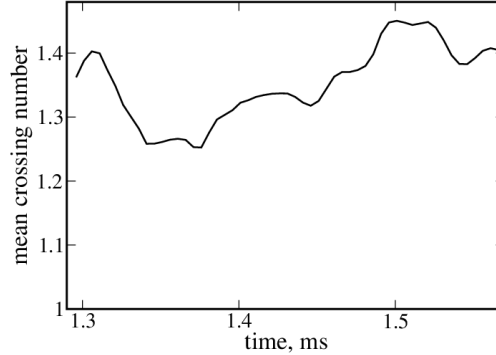
**FIG. 3.** Evolution of turbulent burning velocities evaluated using Eqs. (1) and (2).



158  
159 **FIG. 4.** Contributions of sets of rays, characterized by different  $N_f(y, z, t)$  specified in legends, to bulk  
160 HRR.

161 However, Fig. 4 shows that contributions of folded flame elements, i.e., rays characterized  
162 by  $N_f(y, z, t) \geq 3$ , to volume integrated HRR is rather small, always less than 30%. These  
163 contributions have been evaluated by integrating the HRR along all rays characterized by the  
164 same  $N_f(y, z, t) = \mathbb{N}$  and dividing the sum of these integrals with the number  $N_r(\mathbb{N})$  of such  
165 rays, i.e.,

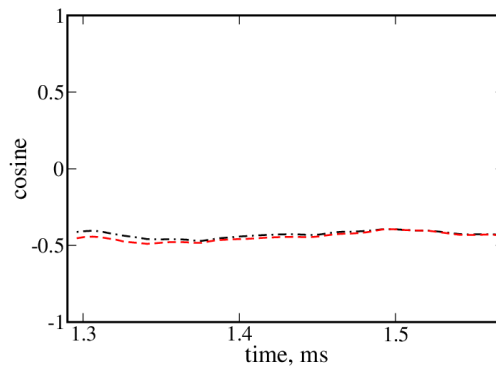
166 
$$U_{\mathbb{N}}^{HRR}(t) = \frac{1}{\rho_u(T_b - T_u)N_r} \sum_{N_f(y,z,t)=\mathbb{N}} [\int \dot{\omega}_T(\mathbf{x}, t) dx]. \quad (3)$$



167  
168 **FIG. 5.** Evolution of volume-averaged crossing number.

169 Besides, the mean crossing number  $\langle N_f \rangle(t)$ , i.e.,  $N_f(y, z, t)$  averaged over all rays, is also  
170 sufficiently small, see Fig. 5, at least, significantly less than  $U_t^{HRR}(t)/S_L$ . These results are  
171 consistent with an earlier DNS study<sup>36</sup> of constant-density highly turbulent reacting waves  
172 characterized by various  $0.01 \leq Da < 1.0$ . That study has shown that an increase in  $U_t(t)/S_L$

173 in a turbulent flow is mainly controlled by inclination of instantaneous flames with respect to  
 174 the normal to the mean flame brush, whereas flame folding plays a secondary role. The  
 175 inclination effect is illustrated in Fig. 6, which reports mean values  $\langle n_x \rangle(t)$  of  $n_x(y, z, t)$   
 176 evaluated in all crossing points for the cold (black dotted-dashed line in Fig. 6 and circles in  
 177 Fig. 1) and hot (red dashed line in Fig. 6 and crosses in Fig. 1) boundaries of reaction zones.  
 178 Here,  $n_x$  is the  $x$ -component of the unit normal vector  $\mathbf{n} = -\nabla c/|\nabla c|$ .

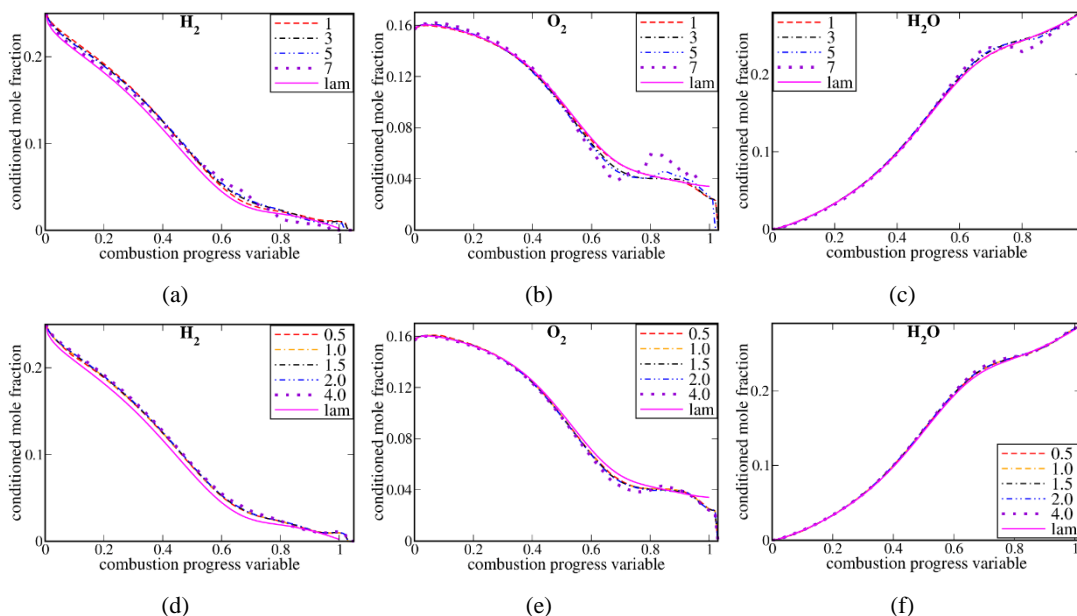


179  
 180 **FIG. 6.** Volume-averaged cosines  $\langle n_x \rangle(t)$  evaluated in all crossing points for the cold (black dotted-  
 181 dashed line) and hot (red dashed line) boundaries of local reaction zones.

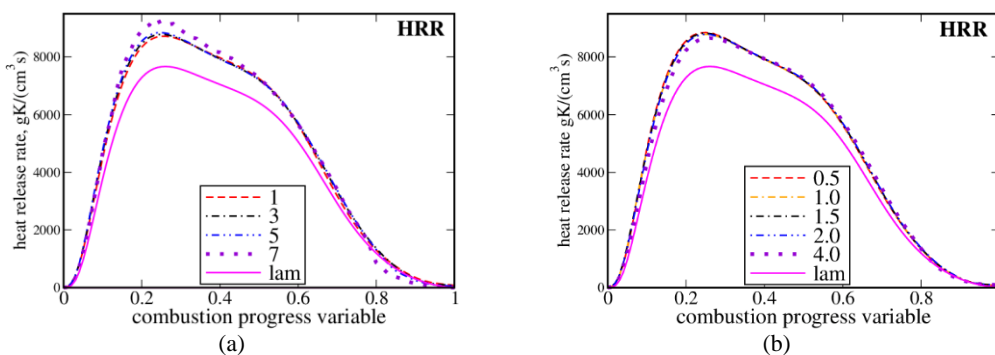
182 Thus, under conditions of the considered DNS, the probability of folding events is  
 183 sufficiently low. Accordingly, the capability of flamelet approach for predicting mean mole  
 184 fractions of various species in the studied flame<sup>14,16</sup> could be attributed to this low probability.  
 185 However, the probability is sufficiently high ( $\approx 20\%$ ) to sample statistics conditioned to  
 186 folding events and to explore the influence of such events on the local flame scalar structure.

187 Figures 7-9 report the conditional profiles  $\langle \phi | \xi, N_m \rangle$  and  $\langle \phi | \xi, \Delta_m \rangle$ , sampled at different  
 188  $N_m$  and  $\Delta_m$ , respectively, for mole fractions ( $\phi = X_i$ ) of  $H_2$ ,  $O_2$ , and  $H_2O$ , HRR ( $\phi = \dot{\omega}_T$ ),  
 189 and rates ( $\phi = \dot{\omega}_i$ ) of consumption of  $H_2$  and  $O_2$  or creation of  $H_2O$ . Simple conditioned  
 190 profiles of  $\langle \phi | \xi \rangle$  are not shown, because they were reported earlier<sup>4,6</sup> and are very close to the  
 191 doubly conditioned profiles for  $N_m = 1$  or  $\Delta_m = 4\delta_L$ . All the conditional profiles, see broken  
 192 lines, are very close to each other and sufficiently close to the counterpart profiles obtained

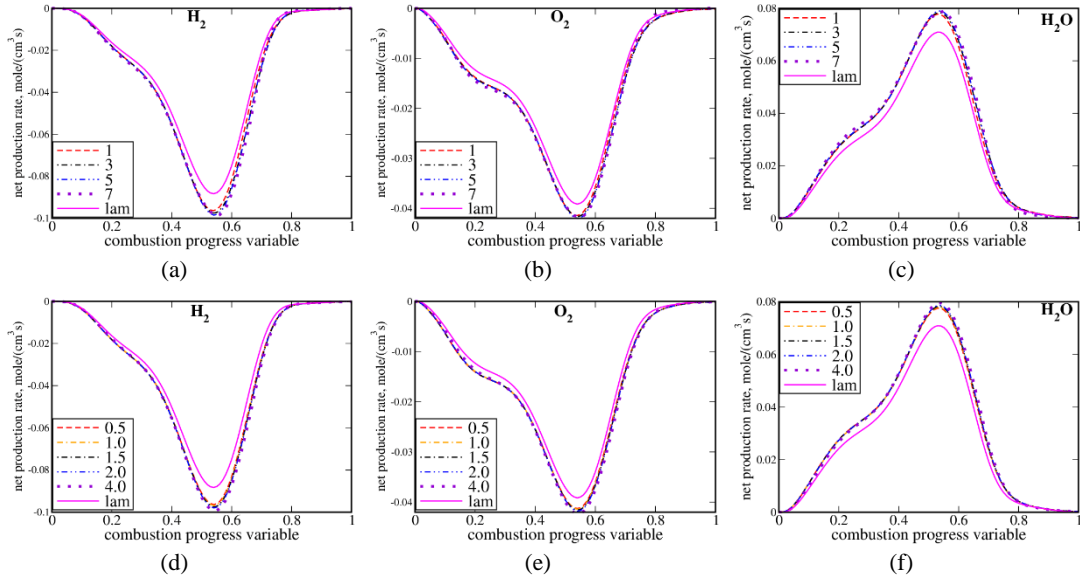
193 from the laminar flame, see solid lines. A weak effect of flame folding on the conditional  
 194 profiles  $\langle \phi | \xi, N_m \rangle$  is observed only for  $N_m = 7$  and only for HRR or mole fractions of  $O_2$  and  
 195  $H_2O$ . Moreover, peak absolute values of the considered rates are lower in the laminar flame,  
 196 but the effect is sufficiently weak.



197 **FIG. 7.** Mole fractions of (a, d)  $H_2$ , (b, e)  $O_2$ , and (c, f)  $H_2O$  conditioned to combustion progress variable  
 198 and either (a)-(c) crossing number  $N_f(y, z, t)$ , i.e.,  $\langle X_i | \xi, N_m \rangle$ , or (d)-(f) distance  $\Delta x(y, z, t)$ , i.e.,  
 199  $\langle X_i | \xi, \Delta_m \rangle$ . Profiles obtained from the laminar flame are plotted in magenta solid lines. Legends in  
 200 panels (a)-(c) and (d)-(f) report  $N_f(y, z, t)$  and  $\Delta_m/\delta_L$ , respectively.

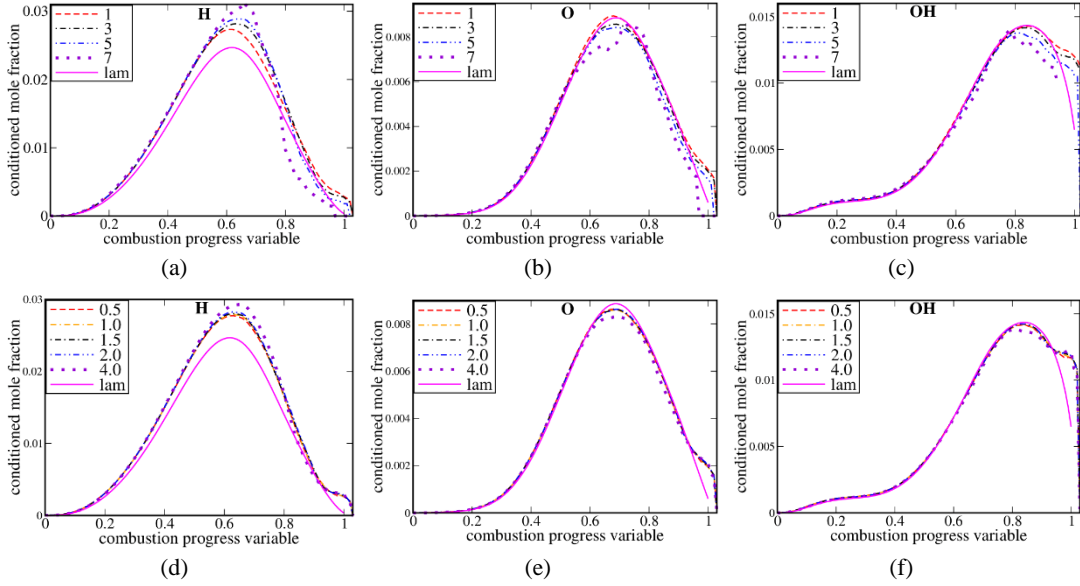


201 **FIG. 8.** Heat release rate conditioned to combustion progress variable and either (a) crossing number  
 202  $N_f(y, z, t)$ , i.e.,  $\langle \dot{\omega}_T | \xi, N_m \rangle$ , or (b) distance  $\Delta x(y, z, t)$ , i.e.,  $\langle \dot{\omega}_T | \xi, \Delta_m \rangle$ . Legends are explained in  
 203 caption to Fig. 7.

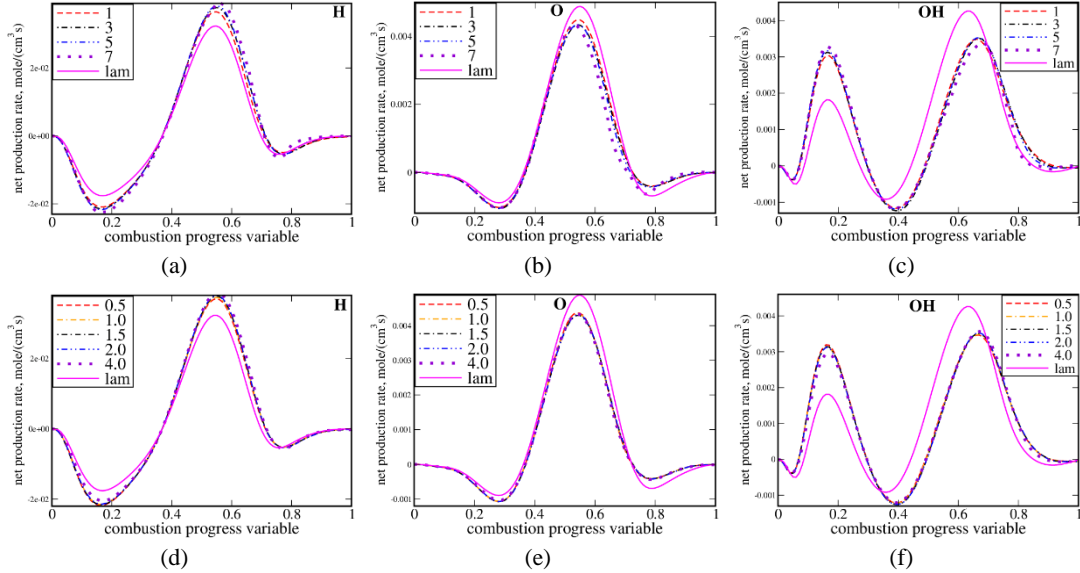


204 **FIG. 9.** Production rates for (a, d)  $\text{H}_2$ , (b, e)  $\text{O}_2$ , and (c, f)  $\text{H}_2\text{O}$  conditioned to combustion progress  
 205 variable and either (a)-(c) crossing number  $N_f(y, z, t)$  or (d)-(f) distance  $\Delta x(y, z, t)$ . Legends are  
 206 explained in caption to Fig. 7.

207 Figures 10-13 show that the doubly conditioned profiles of radical mole fractions and  
 208 production rates are also weakly affected by  $N_m$  or  $\Delta_m$ . While differences between the  
 209 conditional profiles  $\langle X_l | \xi, N_m \rangle$  sampled at different  $N_m$  and the laminar flame profiles  $X_{l,L}(c)$   
 210 are increased with  $N_m$  for mole fractions of H, O, and OH, see Figs. 10a-10c, these differences  
 211 are sufficiently small. For mole fractions of  $\text{HO}_2$  and  $\text{H}_2\text{O}_2$  and for all radical production rates,  
 212 differences between the profiles conditioned to various  $N_m$  or  $\Delta_m$  are significantly less than  
 213 differences between these profiles and the laminar flame profiles. Accordingly, the validity of  
 214 the flamelet paradigm is limited by physical mechanisms associated with perturbations of a  
 215 single local flame (e.g., flame stretching by small-scale turbulent eddies or local variations in  
 216 the equivalence ratio and temperature due to differential diffusion effects<sup>37</sup>), rather than by  
 217 flame folding. For instance, due to the differential diffusion effects, the local combustion  
 218 progress variable can be larger than unity, with differences between the conditional profiles  
 219  $\langle X_l | \xi, N_m \rangle$  sampled at different  $N_m$  and  $X_{l,L}(c)$  being most pronounced at  $c(\mathbf{x}, t) \approx 1$  for  $\text{O}_2$ ,  
 220  $\text{H}_2\text{O}$ , OH, and H, see Fig. 7b, 7c, 10b, and 10c.



221 **FIG. 10.** Mole fractions of the radicals (a, d) H, (b, e) O and (c, f) OH conditioned to combustion  
 222 progress variable and either (a)-(c) crossing number  $N_f(y, z, t)$  or (d)-(f) distance  $\Delta x(y, z, t)$ . Legends  
 223 are explained in caption to Fig. 7.



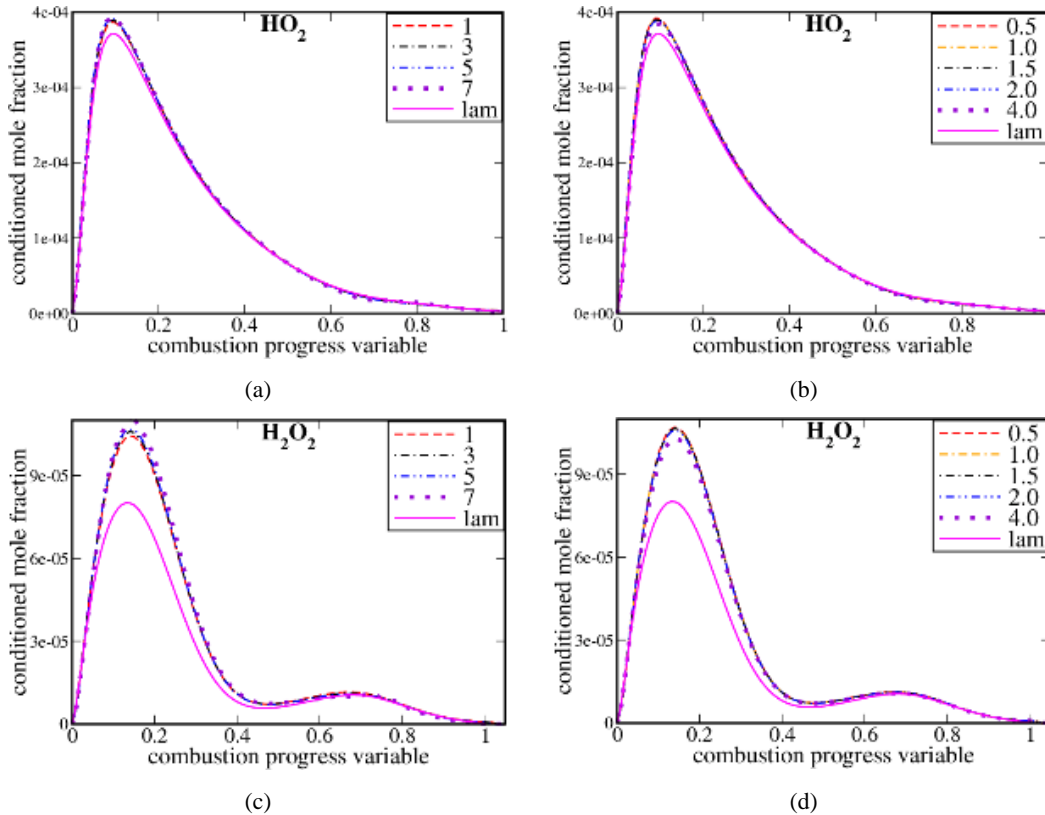
224 **FIG. 11.** Rates of production/consumption of the radicals (a, d) H, (b, e) O and (c, f) OH conditioned  
 225 to combustion progress variable and either (a)-(c) crossing number  $N_f(y, z, t)$  or (d)-(f)  
 226 distance  $\Delta x(y, z, t)$ . Legends are explained in caption to Fig. 7.

227 In this regard, it is worth emphasizing the following two points. First, the present work aims  
 228 mainly at studying the influence of flame holding on the validity of the flamelet paradigm.  
 229 Therefore, comparison of the conditional profiles  $\langle \phi | \xi, N_m \rangle$  sampled at different  $N_m$  or the

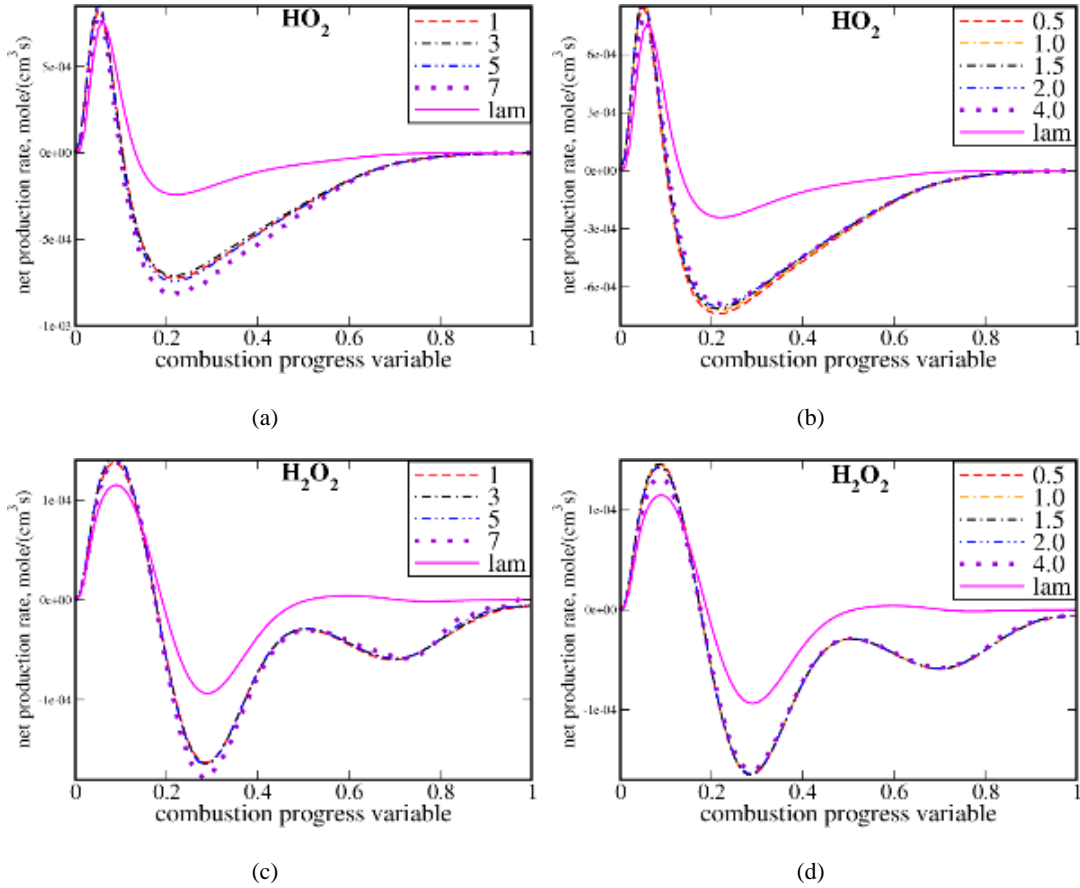
230 conditional profiles  $\langle \phi | \xi, \Delta_m \rangle$  sampled at different  $\Delta_m$  is of primary interest, whereas the  
231 counterpart profiles  $\phi_L(c)$  obtained from the unperturbed laminar flame are solely reported  
232 for illustration. In other words, investigation of the influence of small-scale turbulent eddies  
233 on the simple conditional profiles  $\langle \phi | \xi \rangle$  is beyond the scope of the present work. In intense  
234 turbulence, variations in  $\langle \phi | \xi \rangle$  can stem, e.g., from local strain effects or local intensification  
235 of mixing by small-scale turbulent eddies. Within the framework of the flamelet paradigm,  
236 such effects could be addressed by invoking the profiles  $\phi_L(c)$  obtained from strained laminar  
237 flames or equidiffusive laminar flames, e.g., see recent papers by Skiba et al.<sup>13</sup> and Lipatnikov  
238 et al.,<sup>18</sup> respectively. Eventual influence of flame folding on the validity of so extended  
239 flamelet paradigm should be explored by analyzing DNS data obtained under conditions of  
240 sufficiently intense turbulence and this could be a goal for a subsequent study. Under  
241 conditions of the DNS analyzed here (moderately intense turbulence), the simplest version of  
242 the flamelet paradigm works well. For instance, as discussed in detail elsewhere,<sup>14,16</sup>  
243 dependencies of the mean  $\bar{\phi}$  on the mean  $\bar{c}$  can be well predicted by averaging the profiles  
244  $\phi_L(c)$  obtained from the unperturbed laminar flame. Nevertheless, under these conditions, the  
245 probability of finding large crossing numbers, i.e.,  $N_f(y, z, t) = 3, 5, \text{ or } 7$  is sufficiently large,  
246 because about  $3 \cdot 10^9$  rays can be sampled from 56 snapshots. Therefore, the conditions of  
247 the DNS by Dave et al.<sup>31</sup> fit well to the major goal of the present study, i.e., exploring the  
248 influence of flame folding on the conditional profiles  $\langle \phi | \xi, N_m \rangle$  sampled at  $N_m \geq 3$ .

249 Second, while differential diffusion effects are well known<sup>37</sup> to play an important role in  
250 lean hydrogen-air flames, the equivalence ratio  $\Phi = 0.81$  set by Dave et al.<sup>31</sup> is beyond the  
251 domain of significant statistical importance of these effects. For instance, in a DNS study by  
252 Chen and Im,<sup>38,39</sup> such effects were shown to be weak even at lower  $\Phi = 0.7$ . Statistically  
253 significant differential diffusion effects were not revealed in recent analyses<sup>15,17,40</sup> of other

254 DNS data obtained from lean hydrogen-air flames characterized by  $\Phi = 0.7$ . Moreover, Fig.  
 255 3 shows that turbulent burning velocities evaluated using Eqs. (1) and (2) are very close to  
 256 one another under the present DNS conditions. Since Eq. (2) involves the unperturbed laminar  
 257 flame speed  $S_L$ , Fig. 3 implies that the influence of differential diffusion phenomena on the  
 258 local HRR is statistically weak under the studied conditions. Therefore, eventual interaction  
 259 between flame folding and differential diffusion effects deserves further study by processing  
 260 DNS data obtained from hydrogen-air flames characterized by a substantially lower  
 261 equivalence ratio, e.g.,  $\Phi \leq 0.5$ . Nevertheless, local manifestations of differential diffusion  
 262 effects were documented in the present study, as noted above and below.

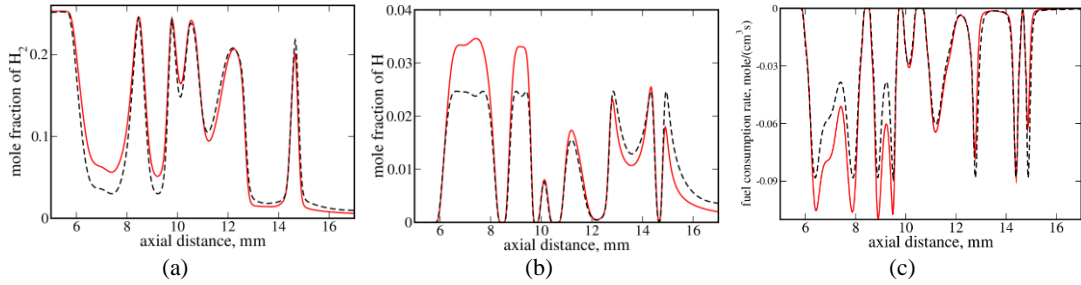


263 **FIG. 12.** Mole fractions of (a, b)  $\text{HO}_2$  and (c, d)  $\text{H}_2\text{O}_2$  conditioned to combustion progress variable and  
 264 either (a, c) crossing number  $N_f(y, z, t)$  or (b, d) distance  $\Delta x(y, z, t)$ . Legends are explained in caption  
 265 to Fig. 7.



266 **FIG. 13.** Production rates of (a, b)  $\text{HO}_2$  and (c, d)  $\text{H}_2\text{O}_2$  conditioned to combustion progress variable  
 267 and either (a, c) crossing number  $N_f(y, z, t)$  or (b, d) distance  $\Delta x(y, z, t)$ . Legends are explained in  
 268 caption to Fig. 7.

269 While flame folding and flame-flame interactions can result in disappearance of some  
 270 segments of the interacting flames, the present results imply that surviving flame segments  
 271 retain their structure to the leading order in the statistical sense. This claim does not mean that  
 272 instantaneous local differences between  $\phi(\mathbf{x}, t)$  in a turbulent flame and  $\phi[c(\mathbf{x}, t)]$  taken from  
 273 simulations of the counterpart laminar flame are always weak. On the contrary, Fig. 14 shows  
 274 that such differences can be significant in the vicinity of the local extreme points of the axial  
 275 profiles sampled from the turbulent flame. Nevertheless, even in this case, the turbulent and  
 276 laminar flame profiles are close at intermediate values of  $c(\mathbf{x}, t)$ .



277 **FIG. 14.** Instantaneous axial profiles of (a) mole fraction of  $H_2$ , (b) mole fraction of  $H$ , and (c) fuel  
 278 production rate, corresponding to the temperature profile plotted in Fig. 2. Red solid lines show profiles  
 279 sampled from the turbulent flame. Black dashed lines show profiles obtained by substituting  $c(x)$   
 280 sampled from the turbulent flame into dependencies of  $\phi_L(c)$  obtained from the laminar flame.

281 Figure 14 also indicates that, in the leading zone ( $x < 10$  mm) of the flame brush, peak  
 282 values of  $|\phi(x) - \phi_u|$  are larger for the turbulent flame profiles of  $X_{H_2}$ ,  $X_H$ , and  $\dot{\omega}_{H_2}$  when  
 283 compared to the flamelet profiles  $\phi_L[c(x)]$ , whereas the opposite trend is observed in the  
 284 trailing zone ( $x > 13$  mm). This observation, which typically holds for many other randomly  
 285 selected axial profiles not reported here for brevity, could be attributed to differential diffusion  
 286 phenomena. Indeed, for lean hydrogen-air flames, (i) such phenomena are known<sup>37</sup> to result  
 287 in increasing (decreasing) the local temperature, equivalence ratio, HRR, and fuel  
 288 consumption rate in positively (negatively, i.e., the curvature center in the unburned reactants)  
 289 curved reaction zones and (ii) such zones are predominately localized to the leading (trailing)  
 290 edge of a premixed turbulent flame brush for purely geometrical reasons, e.g., see Fig. 8b in  
 291 a recent paper by Sabelnikov et al.<sup>40</sup>. Thus, even if differential diffusion phenomena weakly  
 292 affect (for  $\Phi = 0.81$ ) bulk flame characteristics such as  $U_t^{HRR}(t)$ , see Fig. 3, such phenomena  
 293 can play an important role locally.

#### 294 IV. CONCLUSIONS

295 To explore eventual influence of flame folding and flame-flame interactions on the structure  
 296 of local flames in a turbulent flow, new diagnostic techniques were applied to processing DNS  
 297 data obtained from a moderately turbulent, complex-chemistry, lean hydrogen-air flame. The

298 techniques consist of counting crossing numbers  $N_f(y, z, t)$  for a cold boundary of the local  
299 reaction zone and a ray normal to the mean flame brush, followed by analyzing statistics  
300 sampled from rays characterized by  $N_f(y, z, t) \geq 3$ . More specifically, profiles of species  
301 mole fractions, temperature, heat release rate, and species production rates, conditioned to  
302 combustion progress variable and either  $N_f(y, z, t)$  or axial distance between two neighboring  
303 reaction zones, were sampled and compared.

304 Results show that the doubly conditioned profiles are close to each other for various  
305 crossing numbers or for various axial distances even if the distance is as small as half laminar  
306 flame thickness, e.g., see two interacting flames at  $x \approx 14.5$  mm in Fig. 2.

307 The lack of a substantial effect of the crossing number or the axial distance on the doubly  
308 conditioned profiles implies that small-scale flame folding is unlikely to limit validity of  
309 flamelet paradigm, which seems to be controlled by other physical mechanisms (local flame  
310 stretching, differential diffusion, etc.). In the statistical sense, the present results further  
311 support using flamelet paradigm for turbulent combustion modeling. Since this study is  
312 restricted to analyzing a single moderately turbulent flame, application of the developed  
313 diagnostic techniques to other DNS data computed, e.g., at a higher  $u'$  or Karlovitz number,  
314 appears to be of interest and importance. Nevertheless, certain confidence to the major  
315 conclusion regarding weak influence of small-scale flame folding on the flamelet approach  
316 validity is given by the facts that (i) the reported profiles have been conditioned to as large as  
317  $N_f(y, z, t) = 7$  folding events, (ii) some folding events are associated with a highly perturbed  
318 local structure of reaction zones (e.g., see Figs. 2 and 14), but, nevertheless, (iii) the  
319 documented influence of variations in  $1 \leq N_f(y, z, t) \leq 7$  on the conditioned profiles is very  
320 weak.

## 321 **ACKNOWLEDGEMENTS**

322 The authors are very grateful to Swetaprovo Chaudhuri and Himanshu Dave for providing  
323 their DNS data. ANL gratefully acknowledges the financial support provided by Combustion  
324 Engine Research Center (CERC). VAS gratefully acknowledges the financial support  
325 provided by ONERA.

## 326 **AUTHOR DECLARATIONS**

### 327 **Conflict of Interest**

328 The authors have no conflicts to disclose.

## 329 **DATA AVAILABILITY**

330 The data that support the findings of this study are available from the corresponding author  
331 upon reasonable request.

## 332 **REFERENCES**

- 333 <sup>1</sup>R. Yu and A. N. Lipatnikov, “DNS study of dependence of bulk consumption velocity in a constant-  
334 density reacting flow on turbulence and mixture characteristics,” *Phys. Fluids* **29**, 065116 (2017).
- 335 <sup>2</sup>L. Cifuentes, C. Dopazo, A. Sandeep, N. Chakraborty, and A. Kempf, “Analysis of flame curvature  
336 evolution in a turbulent premixed bluff body burner,” *Phys. Fluids* **30**, 095101 (2018).
- 337 <sup>3</sup>A. Y. Klimenko, “The convergence of combustion models and compliance with the Kolmogorov  
338 scaling of turbulence,” *Phys. Fluids* **33**, 025112 (2021).
- 339 <sup>4</sup>T. Readshaw, T. Ding, S. Rigopoulos, and W. P. Jones, “Modeling of turbulent flames with the large  
340 eddy simulation–probability density function (LES–PDF) approach, stochastic fields, and artificial  
341 neural networks,” *Phys. Fluids* **33**, 035154 (2021).
- 342 <sup>5</sup>V. A. Sabelnikov and A. N. Lipatnikov, “Scaling of reaction progress variable variance in highly  
343 turbulent reaction waves,” *Phys. Fluids* **33**, 085103 (2021).
- 344 <sup>6</sup>C. Dopazo, L. Cifuentes, and N. Chakraborty, “Vorticity budgets in premixed combustng turbulent  
345 flows at different Lewis numbers,” *Phys. Fluids* **29**, 045106 (2017).
- 346 <sup>7</sup>A. N. Lipatnikov, V. A. Sabelnikov, S. Nishiki, and T. Hasegawa, “Combustion-induced local shear  
347 layers within premixed flamelets in weakly turbulent flows,” *Phys. Fluids* **30**, 085101 (2018).
- 348 <sup>8</sup>A. N. Lipatnikov, V. A. Sabelnikov, S. Nishiki, and T. Hasegawa, “Does flame-generated vorticity  
349 increase turbulent burning velocity?” *Phys. Fluids* **30**, 081702 (2018).
- 350 <sup>9</sup>P. Brearley, U. Ahmed, N. Chakraborty, and A. N. Lipatnikov, “Statistical behaviours of conditioned  
351 two-point second-order structure functions in turbulent premixed flames in different combustion  
352 regimes,” *Phys. Fluids* **31**, 115109 (2019).
- 353 <sup>10</sup>N. Chakraborty, C. Kasten, U. Ahmed, and M. Klein, “Evolutions of strain rate and dissipation rate  
354 of kinetic energy in turbulent premixed flames,” *Phys. Fluids* **33**, 125132 (2021).
- 355 <sup>11</sup>N. Peters, *Turbulent Combustion* (Cambridge Univ. Press, Cambridge, UK, 2000).

- 356 <sup>12</sup>J. F. Driscoll, J. H. Chen, A. W. Skiba, C. D. Carter, E. R. Hawkes, and H. Wang, “Premixed flames  
357 subjected to extreme turbulence: Some questions and recent answers,” *Prog. Energy Combust. Sci.*  
358 **76**, 100802 (2020).
- 359 <sup>13</sup>A. W. Skiba, C. D. Carter, S. D. Hammack, and J. F. Driscoll, “Experimental assessment of the  
360 progress variable space structure of premixed flames subjected to extreme turbulence,” *Proc.*  
361 *Combust. Inst.* **38**, 2893 (2021).
- 362 <sup>14</sup>A. N. Lipatnikov and V. A. Sabelnikov, “An extended flamelet-based presumed probability density  
363 function for predicting mean concentrations of various species in premixed turbulent flames,” *Int. J.*  
364 *Hydrogen Energy* **45**, 31162 (2020).
- 365 <sup>15</sup>A. N. Lipatnikov, V. A. Sabelnikov, F. E. Hernández-Pérez, W. Song, and H. G. Im, “A priori DNS  
366 study of applicability of flamelet concept to predicting mean concentrations of species in turbulent  
367 premixed flames at various Karlovitz numbers,” *Combust. Flame* **222**, 370 (2020).
- 368 <sup>16</sup>A. N. Lipatnikov and V. A. Sabelnikov, “Evaluation of mean species mass fractions in premixed  
369 turbulent flames: A DNS study,” *Proc. Combust. Inst.* **38**, 6413 (2021).
- 370 <sup>17</sup>A. N. Lipatnikov, V. A. Sabelnikov, F. E. Hernández-Pérez, W. Song, and H. G. Im, “Prediction of  
371 mean radical concentrations in lean hydrogen-air turbulent flames at different Karlovitz numbers  
372 adopting a newly extended flamelet-based presumed PDF,” *Combust. Flame* **226**, 248 (2021).
- 373 <sup>18</sup>A. N. Lipatnikov, T. Nilsson, R. Yu, X.-S. Bai, and V. A. Sabelnikov, “Assessment of a flamelet  
374 approach to evaluating mean species mass fractions in moderately and highly turbulent premixed  
375 flames,” *Phys. Fluids* **33**, 045121 (2021).
- 376 <sup>19</sup>H. C. Lee, P. Dai, M. Wan, and A. N Lipatnikov, “Influence of molecular transport on burning rate  
377 and conditioned species concentrations in highly turbulent premixed flames,” *J. Fluid Mech.* **298**,  
378 A5 (2021).
- 379 <sup>20</sup>H. C. Lee, P. Dai, M. Wan, and A. N Lipatnikov, “Lewis number and preferential diffusion effects in  
380 lean hydrogen–air highly turbulent flames,” *Phys. Fluids* **34**, 035131 (2022).
- 381 <sup>21</sup>M. Pfitzner, “A new analytic pdf for simulations of premixed turbulent combustion,” *Flow Turbul.*  
382 *Combust.* **106**, 1213 (2021).
- 383 <sup>22</sup>M. Hansinger, M. Pfitzner and M. Klein, “Statistical analysis and verification of a new premixed  
384 combustion model with DNS data,” *Combust. Sci. Technol.* **192**, 2093 (2020).
- 385 <sup>23</sup>M. Pfitzner and M. Klein, “A near-exact analytic solution of progress variable and pdf for single-step  
386 Arrhenius chemistry,” *Combust. Flame* **226**, 380 (2021).
- 387 <sup>24</sup>M. Pfitzner and P. Breda, “An analytic probability density function for partially premixed flames with  
388 detailed chemistry,” *Phys. Fluids* **33**, 035117 (2021).
- 389 <sup>25</sup>M. Pfitzner, J. Shin, and M. Klein, “A multidimensional combustion model for oblique, wrinkled  
390 premixed flames,” *Combust. Flame* **241**, 112121 (2022).
- 391 <sup>26</sup>T. Echehki, J. H. Chen, and I. Gran, “The mechanism of mutual annihilation of stoichiometric  
392 premixed methane-air flames,” *Proc. Combust. Inst.* **26**, 855 (1996).
- 393 <sup>27</sup>J. H. Chen, T. Echehki, and W. Kollmann, “The mechanism of two dimensional pocket formation in  
394 lean premixed methane-air flames with implications to turbulent combustion,” *Combust. Flame* **116**,  
395 15 (1999).
- 396 <sup>28</sup>A. Y. Poludnenko and E. S. Oran, “The interaction of high-speed turbulence with flames: Turbulent  
397 flame speed,” *Combust. Flame* **158**, 301 (2011).
- 398 <sup>29</sup>R. A. C. Griffiths, J. H. Chen, H. Kolla, and R. S. Cant, “Three-dimensional topology of turbulent  
399 premixed flame interaction,” *Proc. Combust. Inst.* **35**, 1341 (2015).
- 400 <sup>30</sup>Y. Minamoto, K. Jigjid, R. Igari, and M. Tanahashi, “Effect of flame-flame interaction on scalar PDF  
401 in turbulent premixed flames,” *Combust. Flame*, in press,  
402 <https://doi.org/10.1016/j.combustflame.2021.111660>
- 403 <sup>31</sup>H. L. Dave, A. Mohan, and S. Chaudhuri, “Genesis and evolution of premixed flames in turbulence,”  
404 *Combust. Flame* **196**, 386 (2018).
- 405 <sup>32</sup>H. L. Dave and S. Chaudhuri, “Evolution of local flame displacement speeds in turbulence,” *J. Fluid*  
406 *Mech.* **884**, A46 (2020).
- 407 <sup>33</sup>J. Li, Z. Zhao, A. Kazakov, and F. L. Dryer, “An updated comprehensive kinetic model of hydrogen  
408 combustion,” *Int. J. Chem. Kinetics* **36**, 566 (2004).

- 409 <sup>34</sup>N. Babkovskaia, N. E. L. Haugen, A. Brandenburg, “A high-order public domain code for direct  
410 numerical simulations of turbulent combustion,” *J. Comput. Phys.* **230**, 1 (2011).
- 411 <sup>35</sup>T. J. Poinso and S. K. Lele, “Boundary conditions for direct simulations of compressible viscous  
412 flows,” *J. Comput. Phys.* **101**, 104 (1992).
- 413 <sup>36</sup>V. A. Sabelnikov, R. Yu, and A. N. Lipatnikov, “Thin reaction zones in constant-density turbulent  
414 flows at low Damköhler numbers: Theory and simulations,” *Phys. Fluids* **31**, 055104 (2019).
- 415 <sup>37</sup>A. N. Lipatnikov and J. Chomiak, “Molecular transport effects on turbulent flame propagation and  
416 structure,” *Prog. Energy Combust. Sci.* **31**, 1 (2005).
- 417 <sup>38</sup>J. H. Chen and H. G. Im, “Stretch effects on the burning velocity of turbulent premixed hydrogen-air  
418 flames,” *Proc. Combust. Inst.* **28**, 211 (2000).
- 419 <sup>39</sup>H. G. Im and J. H. Chen, “Preferential diffusion effects on the burning rate of interacting turbulent  
420 premixed hydrogen-air flames,” *Combust. Flame* **131**, 246 (2002).
- 421 <sup>40</sup>V. A. Sabelnikov, A. N. Lipatnikov, S. Nishiki, H. L. Dave, F. E. Hernández-Pérez, W. Song, and H.  
422 G. Im, “Dissipation and dilatation rates in premixed turbulent flames,” *Phys. Fluids* **33**, 035112  
423 (2021).